

## Correlation between texture and formability of aluminum alloy sheets: Crystal plasticity predictions

Mitsutoshi Kuroda, Kengo Yoshida

Graduate School of Science and Engineering, Yamagata University, Jonan 4-3-16, Yonezawa,  
Yamagata 992-8510, Japan

We present our recent achievement of computational studies on improvement of formability of aluminum alloy sheets by texture control. First, the effects of typical texture components (copper, brass, S, cube and Goss) usually observed in rolled aluminum alloy sheets on forming limit strains are numerically studied. It is shown that only the cube texture component yields forming limit strains much higher than those for a random texture in the biaxial stretch range, while the other four texture components tend to yield lower forming limits. Furthermore, it is found that when the orthotropic axes of a material with the cube texture are inclined at  $45^\circ$  relative to the major stretch direction, abnormally high forming limits are obtained for near the in-plane plane strain forming paths, and it is revealed that the emergence of this high formability is attributed to the so-called *geometrical* or *texture hardening* behavior. Next, we seek a possibility for improvement in the formability of aluminum alloy sheets by utilizing the geometrical hardening behavior.

**Keywords:** *Forming limits; Texture; Crystal plasticity; Numerical simulations*

### 1. Introduction

The formability of aluminum alloy sheets is generally poorer than that of standard steel sheets. One of the principal factors that affect the formability of polycrystalline sheets is considered to be the crystallographic texture, and intensive research has been carried out on understanding its influence on the formability of aluminum alloy sheets [1-3]. Effects of some texture components on the forming limits have been investigated by Barlat and Richmond [1] and Ratchev et al. [2]. Their analyses were based on yield loci calculated by Taylor-Bishop-Hill model with initial crystal grain orientations, and thereby changes of the texture during deformation and a *vertex-type* response of plastic strain rate were not taken into account. Recently, using a generalized Taylor-type polycrystal model [3] directly, Wu et al. [4] analyzed the forming limits for a family of the cube textures, which have some orientation scattering around the ideal  $\{100\} \langle 001 \rangle$  orientation. It was found that the cube texture exhibits a significantly high formability in the biaxial stretch range. They, however, discussed only the effect of the cube texture on formability, and influences of the other texture components have not been revealed.

In the present paper, we present our recent achievement of computational studies on improvement of the formability of aluminum alloy sheets by texture control [5, 6]. First, the effects of typical texture components observed in rolled aluminum alloy sheets on forming limit strains are numerically studied. In the analyses, the typical three rolling texture components (copper, brass and S) and typical recrystallization texture components (cube and Goss) are considered. The material response is described by a generalized Taylor-type polycrystal model in which each crystal grain is characterized by an elastic-viscoplastic continuum slip crystal plasticity constitutive relation. It is shown that only the cube texture component yields forming limit strains much higher than those for a random texture in the biaxial stretch range, while the other four texture components tend to yield lower forming limits. Furthermore, it is found that when the orthotropic axes of a material with the cube texture are inclined at  $45^\circ$  relative to the major stretch direction, abnormally high forming limits are obtained for near the in-plane plane strain forming paths, and it is revealed that the emergence of this high formability is attributed to the so-called *geometrical* or *texture hardening*

phenomenon. Next, we seek a possibility for improvement in the formability of aluminum alloy sheets by utilizing the geometrical hardening behavior.

## 2. Procedure of numerical computations

### 2.1 Modeling of textures

In aluminum alloy sheets, the texture typically develops around copper ( $\{112\} \langle 11\bar{1} \rangle$ ), brass ( $\{110\} \langle 1\bar{1}2 \rangle$ ) and S ( $\{123\} \langle 63\bar{4} \rangle$ ) orientations during the rolling process, and around cube ( $\{100\} \langle 001 \rangle$ ) and Goss ( $\{110\} \langle 001 \rangle$ ) orientations during the annealing process. In actual materials, some scattering of grain orientations around the above particular, ideal crystallographic orientations is observed. In the present series of analyses, a misorientation of each grain from the ideal orientation is represented by a rotation tensor  $\mathbf{R}$  that is specified by an arbitrary chosen axis  $\mathbf{a}$  (a unit vector) with an angle  $\omega$ . To generate a texture model that has scattering of grain orientations, the following procedure is repeated until the desired number of grains are obtained: (i) a value of  $\omega$  is taken according to a Gaussian distribution with the mean value of zero and the standard deviation  $\omega_0$ , (ii)  $\mathbf{a}$  is randomly chosen, (iii) the ideal crystal orientation is rotated by  $\mathbf{R}$ , and (iv) the three other equivalent orientations are created at the same time, in order to represent the orthotropic symmetries of the rolled sheet.

### 2.2 Crystal plasticity model

A finite strain crystal plasticity model used here is along the lines presented in Peirce et al. [7]. The slip rate  $\dot{\gamma}^{(\alpha)}$  on the  $\alpha$ th slip system is given by a power law dependence on the resolved shear stress  $\tau^{(\alpha)}$ ,

$$\dot{\gamma}^{(\alpha)} = \dot{\gamma}_0 \operatorname{sgn}(\tau^{(\alpha)}) \left| \tau^{(\alpha)} / g^{(\alpha)} \right|^{1/m}, \quad (1)$$

where  $\dot{\gamma}_0$  is a reference slip rate,  $m$  is a strain rate sensitivity exponent, and  $g^{(\alpha)}$  is a slip system hardness. The evolution law for  $g^{(\alpha)}$  is specified by

$$\dot{g}^{(\alpha)} = h \sum_{\beta} \left| \dot{\gamma}^{(\beta)} \right|, \quad h = h_0 \left( 1 + h_0 \gamma_a / (\tau_0 n) \right)^{n-1}, \quad \gamma_a = \int_0^t \sum_{\alpha} \left| \dot{\gamma}^{(\alpha)} \right| dt, \quad (2)$$

where  $\tau_0$  is the initial value of  $g^{(\alpha)}$ ,  $h_0$  is the initial slip hardening modulus,  $n$  is a power law hardening exponent, and  $t$  is time. An isotropic elasticity is assumed in the present applications, which is determined with the Young's modulus  $E$  and Poisson's ratio  $\nu$ .

As a model for a polycrystal, a Taylor type approach is adopted. The deformation in each grain is taken to be identical to the macroscopic deformation of the aggregate. Taking the volume fraction of each grain to be identical, the macroscopic stress  $\bar{\boldsymbol{\sigma}}$  and macroscopic plastic strain rate  $\bar{\mathbf{D}}^p$  are respectively obtained from averaging the Cauchy stress  $\boldsymbol{\sigma}$  and plastic strain rate  $\mathbf{D}^p$  in each grain over the total number of grains. A macroscopic equivalent plastic strain for polycrystal is defined by

$$\bar{\varepsilon} = \int_0^t \sqrt{(2/3) \bar{\mathbf{D}}^p : \bar{\mathbf{D}}^p} dt. \quad (3)$$

The material parameter values are chosen as  $m = 0.002$ ,  $n = 0.35$ , and  $h_0 / \tau_0 = 9.75$ ,  $E / \tau_0 = 1625$ , and  $\nu = 0.3$ .

### 2.3 Sheet necking analysis

Forming limit strains of textured sheets are analyzed using the Marciniak–Kuczyński (M–K-) type model [8]. A sheet specimen in the  $x_1 - x_2$  plane with a band of initial inhomogeneity in the form of a reduced thickness under the plane-stress assumption is considered (Fig. 1). The rolling direction, RD, and transverse direction, TD, have an angle  $\theta_1$  relative to the  $x_1$  and  $x_2$

directions, respectively. The same texture model is assigned to the two regions inside and outside the imperfection band. In all computations performed here, linear strain paths,

$$\rho = D_{22} / D_{11} = \dot{\epsilon}_{22} / \dot{\epsilon}_{11}, \quad (4)$$

are assumed outside the band, where  $D_{ij}$  are components of the rate of deformation tensor. The range of the strain ratio is taken to be  $-0.5 \leq \rho \leq 1$ . A number of computations are performed with different initial orientations of the imperfection band (here their interval is taken to be  $5^\circ$ ), and the minimum critical major strain is defined as the forming limit strain denoted by  $\epsilon_{11}^*$ . The initial imperfection value, i.e., the ratio of the thickness inside the band to that outside the band, is taken to be 0.999 for all computations in the present paper.

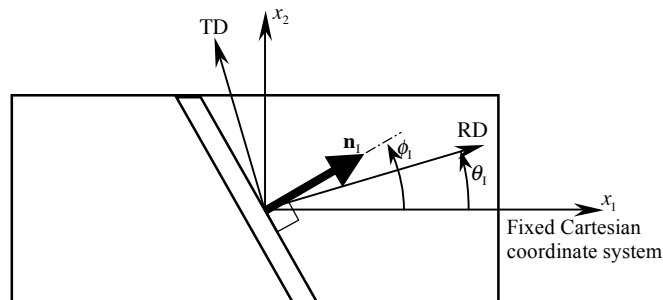


Fig. 1. Textured sheet with orthotropy and an imperfection band with a slightly reduced thickness.

### 3. Influence of the typical texture components on the forming limits

Computed forming limit diagrams (FLDs) for the five texture components with  $\omega_0 = 15^\circ$  are shown in Fig. 2. The  $\omega_0$  of  $15^\circ$  is chosen to represent a realistic scattering of grain orientations around an ideal orientation. In the case where the RD coincides with the  $x_1$ -direction (i.e.  $\theta_1 = 0^\circ$ ) only the cube texture gives formability significantly greater than that for the random texture in the biaxial stretch region ( $\rho > 0$ ) as shown in Fig. 2(a). All the other textures yield poorer stretchability in comparison to that for the random texture. In the in-plane plane strain mode ( $\rho = 0$ ), the limit strain for the cube texture is almost the same as that for the random one. Formability at  $\rho = 0$  is particularly important, because many failures often occur at strain paths near  $\rho = 0$  in stamping operations of automotive panels [9]. Fig. 2(b) shows FLDs when  $\theta_1 = 45^\circ$ . For this orientation, the cube texture produces abnormally higher forming limits in the region  $-0.25 \leq \rho \leq 0.75$ . Indeed, the limit strain  $\epsilon_{11}^*$  of the cube texture for  $\theta_1 = 45^\circ$  is 1.6 times greater than that for  $\theta_1 = 0^\circ$ .

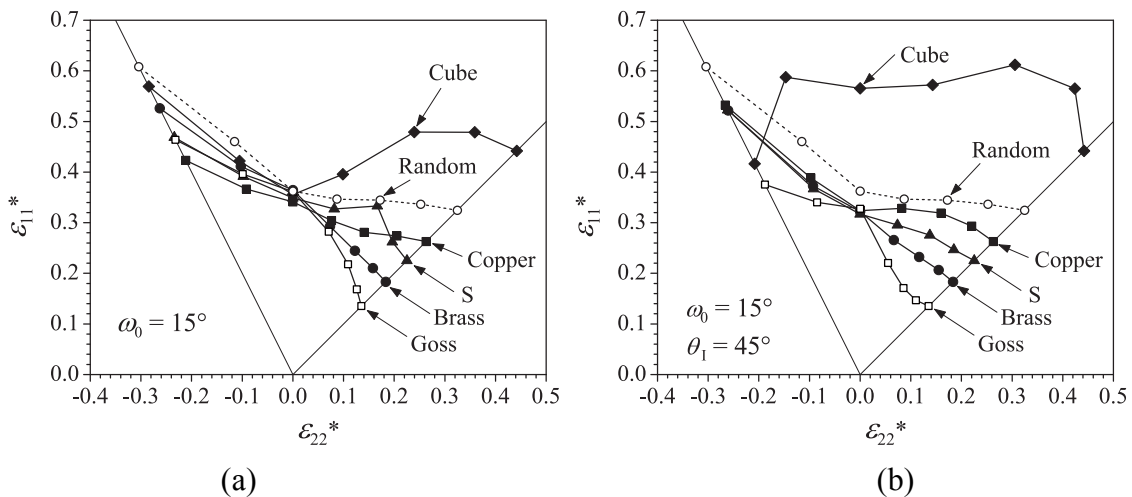


Fig. 2. Computed forming limit diagrams for the five textures with  $\omega_0 = 15^\circ$ : (a)  $\theta_1 = 0^\circ$ ; (b)  $\theta_1 = 45^\circ$ .

For the in-plane plane strain mode ( $\rho=0$ ), forming limit strains primarily depend on the work-hardening behavior: i.e. the higher the work-hardening rate, the higher the forming limit strain. Curves of amounts of normalized work-hardening rate  $H / \bar{\sigma}_{0.2}$  versus tensile strain  $\varepsilon_{11}$  for the case of  $\theta_1 = 45^\circ$  are depicted in Fig. 3. Here,  $H$  is a slope of  $\bar{\sigma}_{11} - \varepsilon_{11}$  curve under the strain mode  $\rho = 0$ , and  $\bar{\sigma}_{0.2}$  represents the value of  $\bar{\sigma}_{11}$  at  $\bar{\varepsilon} = 0.002$ . The value of  $H / \bar{\sigma}_{0.2}$  for the cube texture is clearly higher than those for the other textures. Since we have assumed the same slip hardening law and the same material parameter values for all the textures, this enhanced hardening behavior can be attributed to the so-called *geometrical* (or texture) hardening that is caused by rotations of crystal grains.

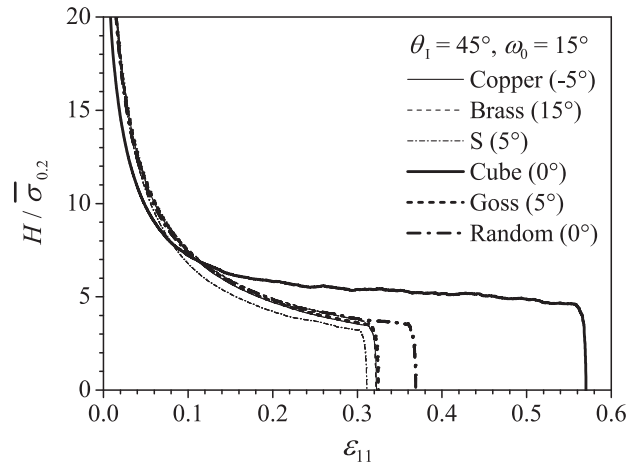


Fig. 3. Relationships between  $H / \bar{\sigma}_{0.2}$  and  $\varepsilon_{11}$  at  $\rho = 0$  for  $\theta_1 = 45^\circ$ .

#### 4. Possibility of improvement in the formability of aluminum alloy sheets by geometrical hardening

As shown in the previous section, the cube texture exhibits a significant geometrical hardening under the in-plane plane strain mode ( $\rho = 0$ ), when  $\theta_1 = 45^\circ$ . Here, stress-strain relations at  $\rho = 0$  are computed for all possible crystal orientations, in order to seek specific orientations that lead to a high degree of geometrical hardening. To keep the orthotropy, each computational model consists of the corresponding four equivalent orientations. In this set of computations, no material hardening ( $h_0 = 0$  MPa) is assumed. Thus, variations of the macroscopic flow stress are solely responsible for the geometrical hardening (or maybe softening). The in-plane plane strain stretching up to  $\bar{\varepsilon} = 1.0$  is applied to each four grain model for the cases of  $\theta_1 = 0^\circ, 22.5^\circ, 45^\circ$ . As a result, the maximum value of  $\bar{\sigma}_{11} / \bar{\sigma}_0$  is found to be 1.6 for a model with an orientation  $(\Psi, \Theta, \Phi) = (63^\circ, 67^\circ, 5^\circ)$  (the Roe angle is used here) stretched in the direction of  $\theta_1 = 0^\circ$ . Here  $\bar{\sigma}_0$  is the stress  $\bar{\sigma}_{11}$  at  $\bar{\varepsilon} = 0.01$ . The second largest  $\bar{\sigma}_{11} / \bar{\sigma}_0$  is 1.4, which appears near the cube orientation, when  $\theta_1 = 45^\circ$ . But, the ideal cube orientation itself yields no geometrical hardening (i.e.  $\bar{\sigma}_{11} / \bar{\sigma}_0 = 1.0$ ). Using the procedure described in Section 2.1, textures developed around  $(\Psi, \Theta, \Phi) = (63^\circ, 67^\circ, 5^\circ)$  and around the cube orientation with scattering according to  $\omega_0 = 5^\circ, 15^\circ$  are created. Each texture model consists of 2000 discrete orientations. The computed stress-strain relations under the in-plane plane-strain stretching is shown in Fig. 4. For the texture developed at  $(\Psi, \Theta, \Phi) = (63^\circ, 67^\circ, 5^\circ)$ , the normalized flow stresses  $\bar{\sigma}_{11} / \bar{\sigma}_0$  at  $\varepsilon_{11} = 1.0$  are 1.6, 1.47 and 1.28 for  $\omega_0 = 0, 5$  and  $15^\circ$ , respectively. The geometrical hardening rapidly decreases with increasing  $\omega_0$ . On the other hand, the cube textures having scattering of orientations with  $\omega_0 = 5^\circ$  and  $15^\circ$  produce a strong geometrical hardening, although the ideal cube ( $\omega_0 = 0^\circ$ ) yields no hardening. Thus, the ideal cube orientation has played no role in the abnormally high formability for  $\theta_1 = 45^\circ$ , which is observed in Fig. 2(b), and the high limit strain is attributed to orientations *around* the ideal cube.

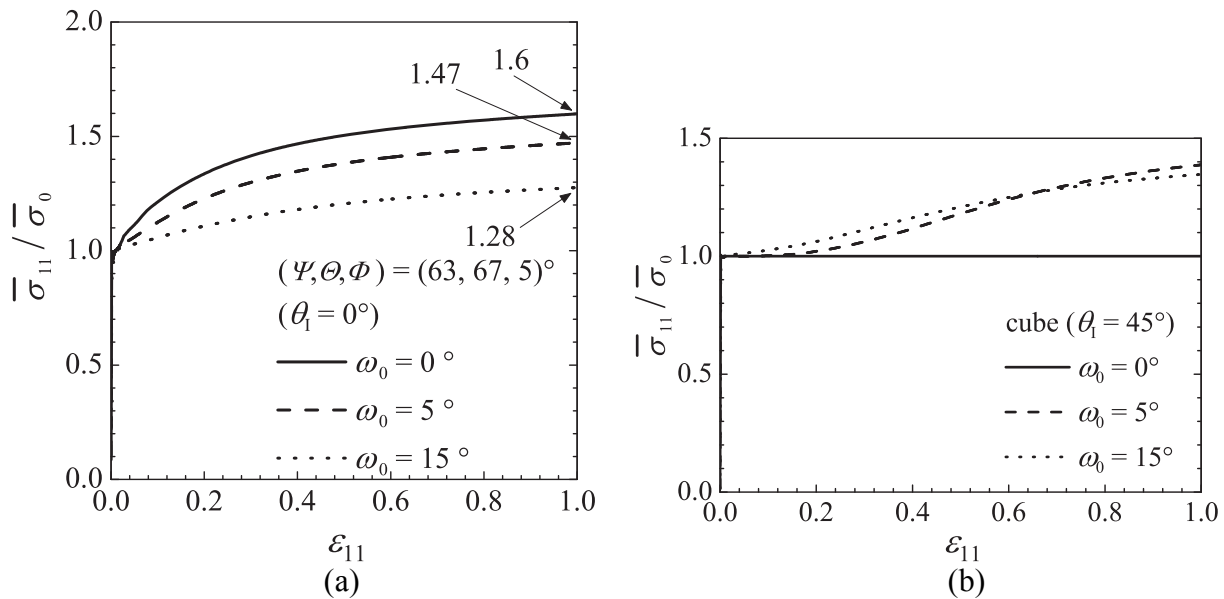


Fig. 4. Geometrical hardening behavior in in-plane plane strain stretching: (a) texture developed at  $(\Psi, \Theta, \Phi) = (63^\circ, 67^\circ, 5^\circ)$  with  $\theta_1 = 0^\circ$ ; (b) cube texture with  $\theta_1 = 45^\circ$ .

As shown in Fig. 4(b), the cube textures with scattering of orientations exhibit the significant amounts of geometrical hardening under the in-plane plane strain mode ( $\rho = 0$ ) when the orthotropic axis is oriented at  $45^\circ$  relative to the tensile axis (i.e.  $\theta_1 = 45^\circ$ ). They, however, does not yield any geometrical hardening for  $\theta_1 = 0^\circ$ . Such strong anisotropy may be unfavorable in industrial productions. A sheet metal that has a texture with in-plane isotropy and sufficient amounts of geometrical hardening for any direction in in-plane stretch might be attractive. Based on the results of the present investigation, we propose the *ND rotated cube texture* that consists of scattered cube textures that are rotated about ND. The  $\{111\}$  pole figure and the geometrical hardening behavior for the ND rotated cube texture are depicted in Fig. 5. The predicted stress–strain curves for  $\omega_0 = 5^\circ$  and  $15^\circ$  are almost identical. Such a small amount of scattering of orientations (i.e.  $\omega_0 \approx 5^\circ$ ) yields the sufficient amount of the geometrical hardening.

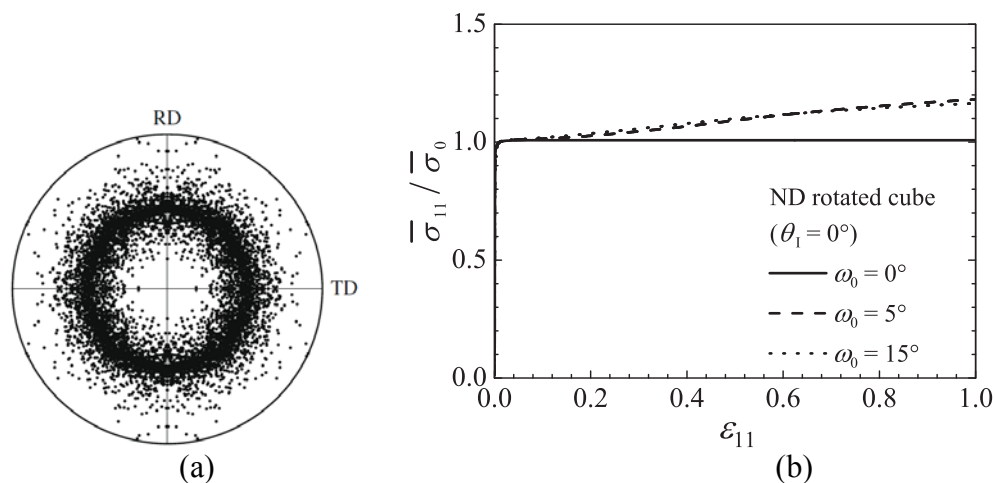


Fig. 5. (a)  $\{111\}$  pole figure of computationally generated ND rotated cube texture ( $\omega_0 = 5^\circ$ , 2000 grains); (b) geometrical hardening behavior of ND rotated cube texture

The FLD for the ND rotated cube texture with  $\omega_0 = 15^\circ$  is shown in Fig. 6, together with FLDs for the random texture and the cube texture for  $\theta_1 = 0^\circ$  and  $45^\circ$ . In these computations, texture models with 2000 grains are used. The limit strains for the ND rotated cube texture are higher than

those for the random and for the cube texture with  $\theta_1 = 0^\circ$  in the whole range of strain paths ( $-0.5 \leq \rho \leq 1.0$ ). Since the ND rotated cube texture has in-plane isotropy, the FLDs for any values of  $\theta_1$  are identical. The limit strain for the ND rotated cube at  $\rho = 0$  is, however, 20% lower than that for the cube texture with  $\theta_1 = 45^\circ$ .

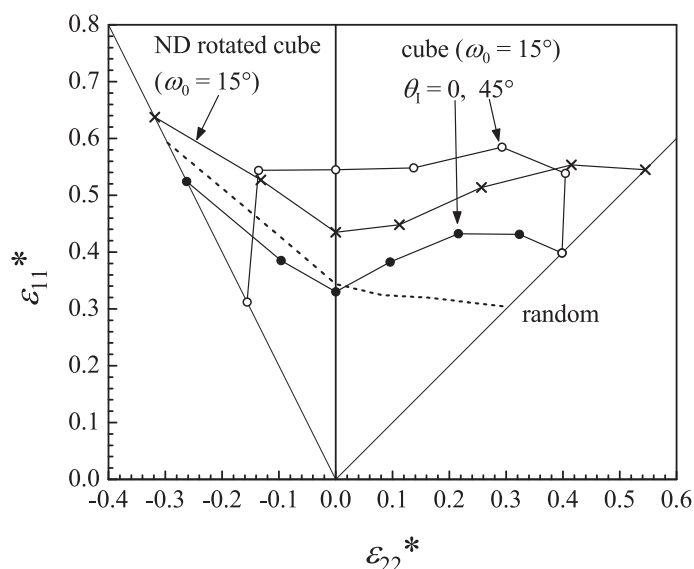


Fig. 6. Forming limit diagrams for the ND rotated cube, random and cube textures.

## 5. Concluding remarks

In the present paper, it has been shown that only the cube texture component yields forming limit strains much higher than those for a random texture in the biaxial stretch range, while the other four texture components tend to yield lower forming limits, and that when the orthotropic axes of the cube texture material are inclined at  $45^\circ$  relative to the major stretch direction, abnormally high forming limits are obtained for near the in-plane plane strain forming paths. The emergence of this high formability is attributed to the so-called *geometrical* or *texture hardening*. Secondly, we have presented a possibility of improvement in the formability of aluminum alloy sheets by utilizing the geometrical hardening behavior. We have demonstrated that the ND rotated cube texture, which has in-plane isotropy, yields high forming limit strains for the whole range of biaxial strain paths.

## References

- [1] F. Barlat, O. Richmond: Mater. Sci. Eng. 95 (1987) 15-29.
- [2] P. Ratchev, P. Van Houtte, B. Verlinden, P. De Smet, P. Neutjens, R. Baartman, P. Drent: Textures and Microstructures 22 (1994) 219-231.
- [3] R.J. Asaro, A. Needleman: Acta Metall. 33 (1985) 923-953.
- [4] P.D. Wu, S.R. MacEwen, D.J. Lloyd, K.W. Neale: Mater. Sci. Eng. A364 (2004) 182-187.
- [5] K. Yoshida, T. Ishizaka, M. Kuroda, S. Ikawa: Acta Mater. 55 (2007) 4499-4506.
- [6] K. Yoshida, Y. Tadano, M. Kuroda: Comput. Mater. Sci. 46 (2009) 459-468.
- [7] D. Peirce, R.J. Asaro, A. Needleman: Acta Metall. 31 (1983) 1951-1976.
- [8] M. Kuroda, V. Tvergaard: Int. J. Solids Struct. 37 (2000) 5037-5059.
- [9] H. Ishigaki: Deformation analysis of large sized panels in the press shop (In: D.P. Koistinen, N.M. Wang, (Eds.), Mechanics of Sheet Metal Forming, Plenum Press, New York, 1978) pp. 315-339.